



http://pubs.acs.org/journal/acsodf

Temperature Dependence of the Artificial Photosynthesis Reactions Catalyzed by Nanostructured Co/CoO

Haizhou Ren, Zhe Kan, Zibo Wang, and Mengyan Shen*



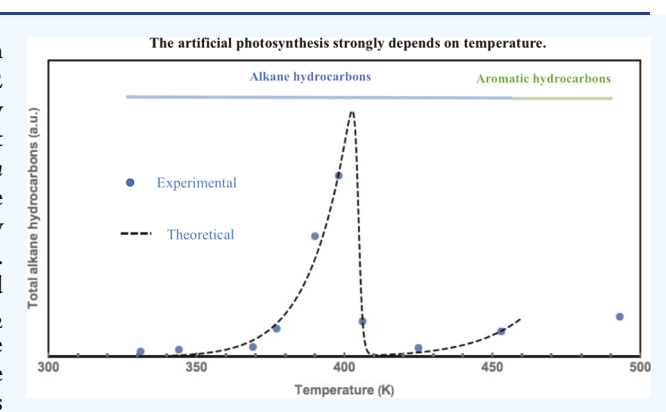
Cite This: https://dx.doi.org/10.1021/acsomega.0c04693



ACCESS

Metrics & More

ABSTRACT: Carbon dioxide (CO_2) and water (H_2O) have been converted into hydrocarbons at temperature ranging from 58 to 242 °C through an artificial photosynthesis reaction catalyzed by nanostructured Co/CoO. The experimental results show that chain hydrocarbons (alkane hydrocarbons) (C_nH_{2n+2}) , where $3 \le n \le 16$) mainly form at a temperature higher than about 60 °C, the production rate reaches a maximum at 130 °C, and abruptly decreases above 130 °C, and then gradually increases until 220 °C. While the temperature is higher than 220 °C, benzene (C_6H_6) and its derivatives such as toluene (C_7H_8) , p-xylene (C_8H_{10}) , and C_9H_{12} form. The modeling of temperature dependence of the reaction rate reveals that the vaporization of the adsorbed water contributes to the sharp peak; the activation energy is estimated as about 1 eV, which is in agreement with the reaction of CO and H_2 to synthesize chain



Article Recommendations

hydrocarbons. The experimental results support the mechanism that the chemisorbed CO_2 and physisorbed H_2O on the CoO surface are disassociated or excited with light, and the disassociated or excited molecules then synthesize hydrocarbons. When most of the water molecules leave from the CoO at temperature higher than $220\,^{\circ}C$, the hydrogen source is of very low concentration while the carbon source remain the same because of the chemisorption, and thus benzene and its derivatives with low hydrogen atom number form.

1. INTRODUCTION

Long-chain hydrocarbons have been synthesized from CO₂, water, and visible light with a nanostructured Co/CoO catalyst at lower temperature and pressure than in previous works. 1-5 The chemisorbed CO₂ molecules and physisorbed H₂O molecules on the surface of the catalyst have found to act as a source of carbon and a source of hydrogen, respectively.³ A mechanism of surface plasmon excitation focusing was proposed, where the intensity of the sunlight is greatly enhanced around the tips of the Co/CoO nanostructures. The enhanced photons dissociate the CO2 and water molecules, and the dissociated molecules synthesize hydrocarbons on the Co/CoO surfaces. 1,2,6,7 The lowest unoccupied molecular orbital (LUMO) of the adsorbed CO₂ has been found to be near to the bottom of the conduction band of CoO, which plays an important role in the dissociation of CO2.3 The carbon isotope effects in the artificial photosynthesis reactions catalyzed by a nanostructured Co/CoO support that when sunlight irradiates the nanostructured surface, electrons may be excited from a defect energy level to the conduction band of CoO and then quantum mechanically tunnel to the LUMO of the CO2 molecules through the plasmonic nano-focusing at the interface.^{3–5} On the other hand, the plasmon-induced hot electrons in Co may

also inject into the conduction band of CoO and then quantum mechanically tunnel to the LUMO energy levels of CO_2 molecules.^{3–5} Then, CO_2 molecules become charged molecules $(CO_2)^-$, which are not stable. An electron is excited from the valence band of CoO to the CoO defect states^{3,4} that are above the valence band on top of CoO. The generated hole in the valence band of CoO then transfers to the highest occupied molecular orbital (HOMO) of the adsorbed H_2O molecules that are on the surface of CoO, which results in $(H_2O)^+$.^{8–13} Since the excited $(CO_2)^-$ and $(H_2O)^+$ molecules are unstable, they synthesize chain hydrocarbons (C_nH_{2n+2}) , where $3 \le n \le 16$) on the CoO catalyst surfaces.^{1–5} The excited $(CO_2)^-$ and $(H_2O)^+$ molecules may also further dissociate to form CO and H_2 .

The thermodynamics of the adsorbed H_2O and CO_2 molecules on the Co/CoO surfaces play an important role in

Received: September 23, 2020 Accepted: November 13, 2020



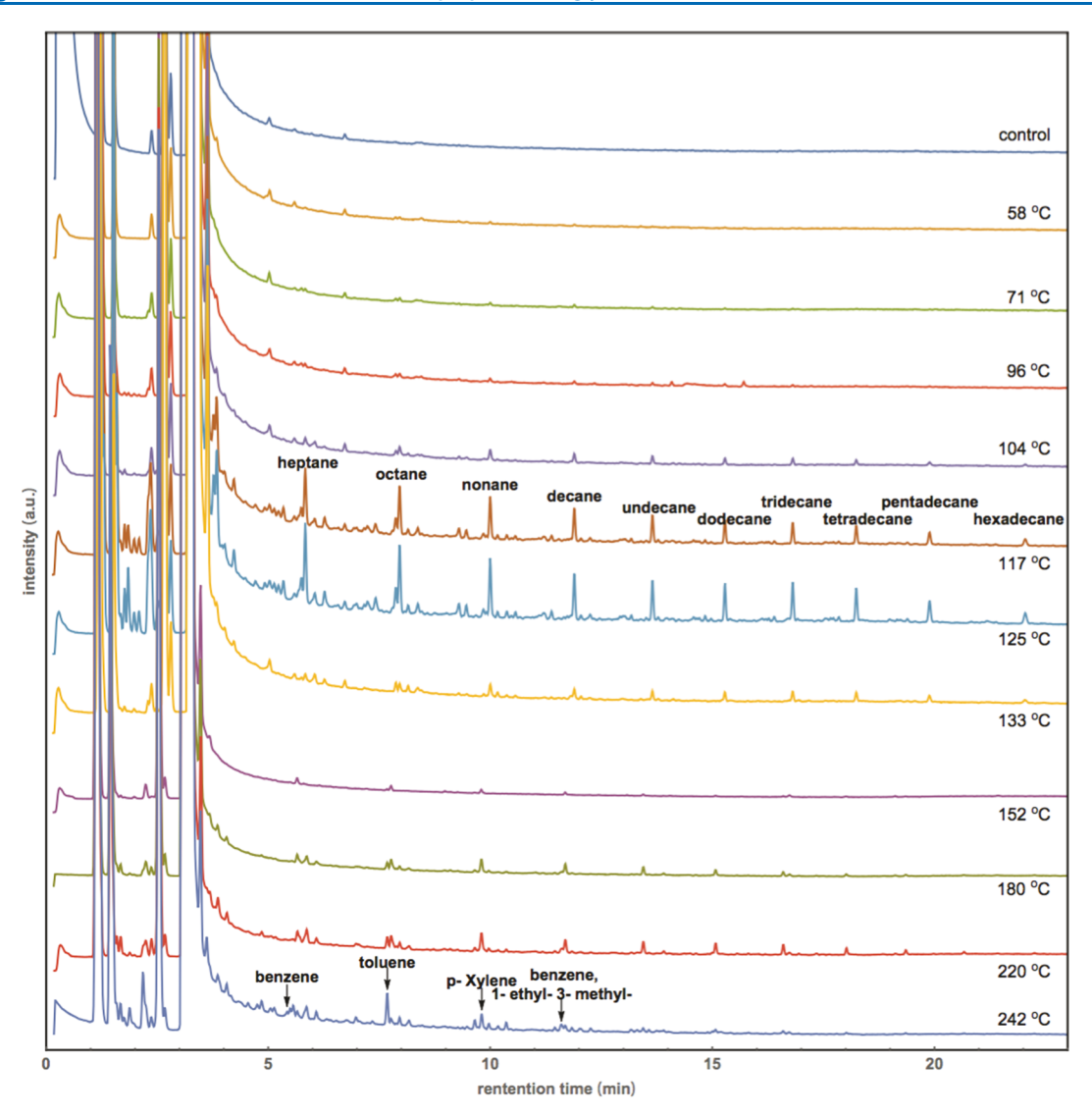


Figure 1. Gas chromatography of products obtained at different temperatures.

the process of artificial photosynthesis.³ Temperature influences the reaction rate for the hydrocarbon syntheses as well as the sources of carbons and hydrogen. However, we did not perform detailed experiment on the temperature influence. In previous experiments, 1-5 we simply set the reactors under the irradiation in an environment at room temperature and neglected the detailed temperature on the Co/CoO surfaces. To further understand the mechanism of the artificial photosynthesis reactions catalyzed by nanostructured Co/ CoO, we perform experiments to investigate the temperature dependence of the hydrocarbon products from 50 to 250 °C at the Co/CoO surfaces. The experimental results show a strong temperature dependence, and the explanation and analysis to the dependence support the mechanism that the chemisorbed CO2 and physisorbed H2O on the CoO surface are disassociated or excited with light; the disassociated or excited molecules then synthesize chain hydrocarbons (C_nH_{2n+2} , where $3 \le n \le 16$) starting from 60 to 220 °C. When most of the water molecules leave from the CoO at a temperature higher than 220 °C, the hydrogen source is of very low concentration, while the carbon source remains the same because of the chemisorption. This may result in that benzene and its derivatives with low hydrogen atom number tend to form.

2. RESULTS AND DISCUSSION

In the control sample, there are peaks of solvent, stabilizer in the solvent, water, gases, and three contaminations from the solvent. Nothing else was shown on the GC graph as shown in the GC spectrum in Figure 1. This confirms that there is no contamination from cobalt, water, or CO₂. The products have found to contain C3 to C17 alkanes and some alcohols. 1-5 Figure 1 shows the GC spectra of products obtained from the experiment at different temperatures. The corresponding GC peaks are labeled in the spectra in Figure 1. The GC peaks of the hydrocarbons whose carbon atom number is less than 7 are overlapped with the solvent peak; however, we can identify them from the MS spectrum. When the temperature is less than 220 °C, the products are mainly chain hydrocarbons. 1-5 Trace amounts of hydrocarbons start to show up in the sample obtained at the 58 °C. When the temperature rises, the production rate gradually increases. At 125 °C, the production rate reaches the maximum. Around the main alkane peaks, there are some sub-peaks from alkenes and isomers of the main products. After the temperature reaches higher than 125 °C, the production decreases quickly.

The individual hydrocarbon peak intensity in the CG spectra is proportional to its molar amount, and the individual

products are extracted from the GC spectra. Figure 2 shows the detailed temperature dependence of individual hydro-

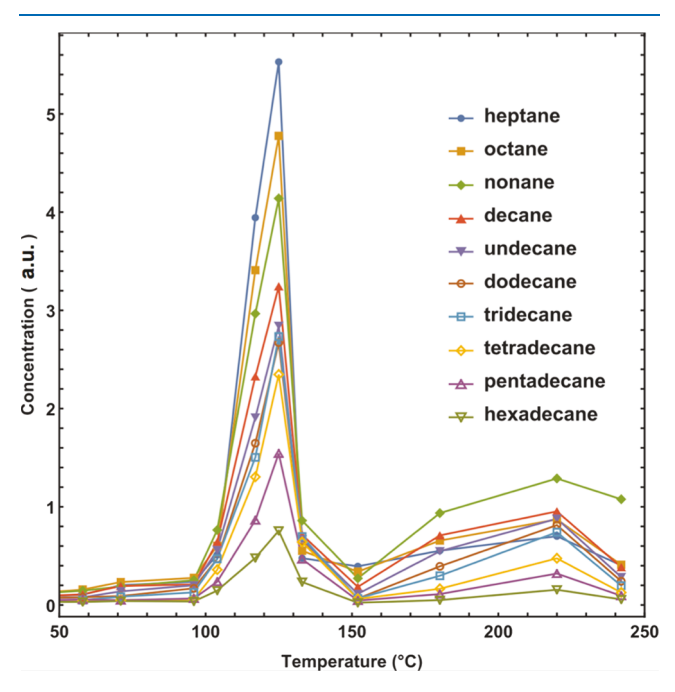


Figure 2. Temperature dependence of alkane hydrocarbon production.

carbon chains. All the products show almost the same temperature dependence. The products increase very slowly below 100 °C. When the temperature approaches 100 °C, the production rate increases rapidly, and all of the products reach the peak value at 125 °C. Its production rate increased by more than 20 times from 90 to 125 °C. While the temperature rises higher than 125 °C, the production suddenly decreases until 150 °C, then increases until 220 °C, then the chain hydrocarbons decrease as the temperature increase further. The MS in Figure 3 shows that when the temperature is higher than 220 °C, benzene (C_6H_6) and its derivatives such as toluene (C_7H_8), *p*-xylene (C_8H_{10}), and C_9H_{12} form. C_9H_{12} cannot be identified as benzene 1-ethyl-3-methyl- or other C_9H_{12} benzene derivatives because their MS spectra are similar. ¹⁴

High-precision detection indicates trace amounts of CO in the photosynthesis process. ¹⁵ Some oxygen was detected with an O_2 detector, although the precision was too low to quantify the detail, and further analysis using a gas chromatograph equipped with thermal conductivity detectors (GC-TCD) also revealed trace amounts of H_2 . This is in agreement with the well-known water spitting process with photons and metal oxides. For example, CoO. CoO/Co can also be used for splitting water. ^{1–5} These observations support the existence of intermediate photodissociation processes where excited states or radicals are formed:

$$H_2O + photons \rightarrow (H_2)^* + \frac{1}{2}O_2$$
 (1)

$$CO_2$$
 + photons \rightarrow $(CO)^* + \frac{1}{2}O_2$ (2)

()* stands for an excited state. Hydrocarbons will form as soon as $(H_2)^*$ and $(CO)^*$ are produced on the surface of CoO:

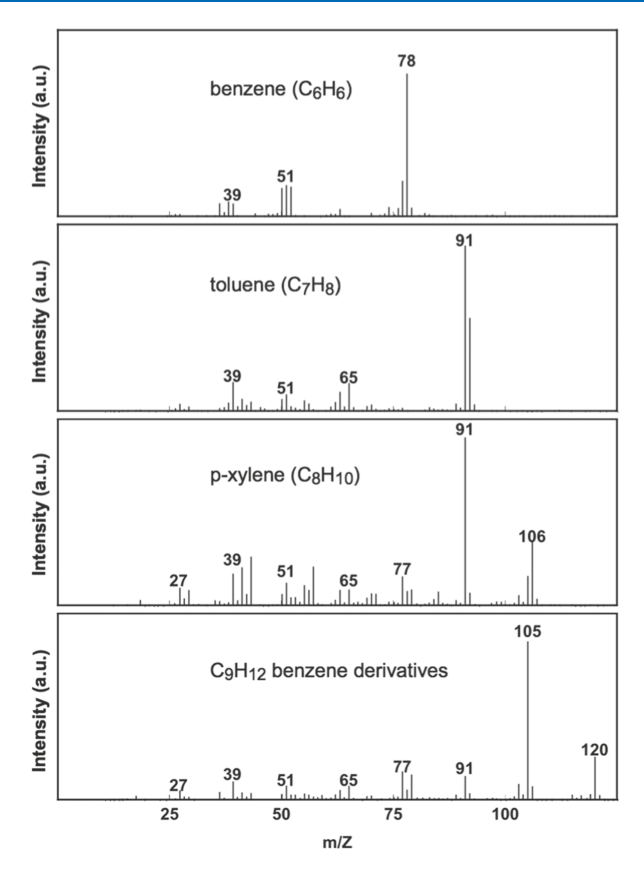


Figure 3. MS spectra of benzene (C_6H_6) , toluene (C_7H_8) , and p-xylene (C_8H_{10}) and C_9H_{12} benzene derivatives from the products at 242 °C.

$$(2n+1)(H_2)^* + n(CO)^* \rightarrow C_n H_{(2n+2)} + nH_2O$$
 (3)

Only small amounts of $(H_2)^*$ and $(CO)^*$ may remain as detectable carbon monoxide and hydrogen gases since they are consumed in the hydrocarbon synthesis.³ The reaction rate may be found to have the form ¹⁶

$$r = k(T)[(H_2)^*]^m[(CO)^*]^l$$
(4)

Here, k(T) is the reaction rate constant that depends on temperature, and $[(H_2)^*]$ and $[(CO)^*]$ are the concentrations of substances $(H_2)^*$ and $(CO)^*$, respectively, in molecular number per unit area of the CoO/O surface solution, assuming the reaction is taking place on the surface. The exponents m and l are called partial orders of reaction and are not generally equal to the stoichiometric coefficients (2n+1) and n. Instead, they depend on the reaction mechanism and can be determined experimentally. The Arrhenius equation gives the dependence of the rate constant of the chemical reaction on the temperature, 17

$$k(T) = Ae^{-(E_{\rm a}/k_{\rm B}T)} \tag{5}$$

A is the pre-exponential factor, a constant for each chemical reaction. According to the collision theory, A is the frequency of collisions in the correct orientation, and $E_{\rm a}$ is the activation energy for the reaction. $k_{\rm B}$ is the Boltzmann constant.

The adsorbed CO_2 and H_2O molecules on the CoO surfaces are the sources of carbons and hydrogen in the process of artificial photosynthesis, respectively. CO₂ molecules are mainly chemisorbed on the CoO surfaces, and H_2O molecules are mainly physisorbed on the CoO surfaces. Chemisorbed CoO surfaces.

isorption may increase with increased temperature, while physisorption decreases with increased temperature. H_2O molecules are less likely to be absorbed when they are in the gas phase than in the liquid phase, 19,20 and this decrease in physisorption greatly reduces effective amount of reactants and thus bottlenecks the reaction rate. Using the vapor pressure as a function of temperatures 21 and estimating the reaction chamber pressure as a function of temperature, we obtain a critical temperature $T_{\rm v}$ at which water has a phase transition. The hydrogen source greatly decreases above $T_{\rm v}$, according to eq 4, we will have thus an abrupt decrease in the reaction rate.

In the experiment, at about 20 °C, the reaction chamber is filled to an absolute pressure of 2 atm. The reaction chamber is a closed system; when the temperature increases to about 100 °C, the pressure in the chamber would rise to 2.5 atm. The vapor pressure of water increases with its temperature; when the pressure in the action chamber is lower than the vapor pressure, most of the adsorbed $\rm H_2O$ molecules will desorb from the CoO surface. The pressure in the chamber can be calculated with the state equation of an ideal gas as shown in

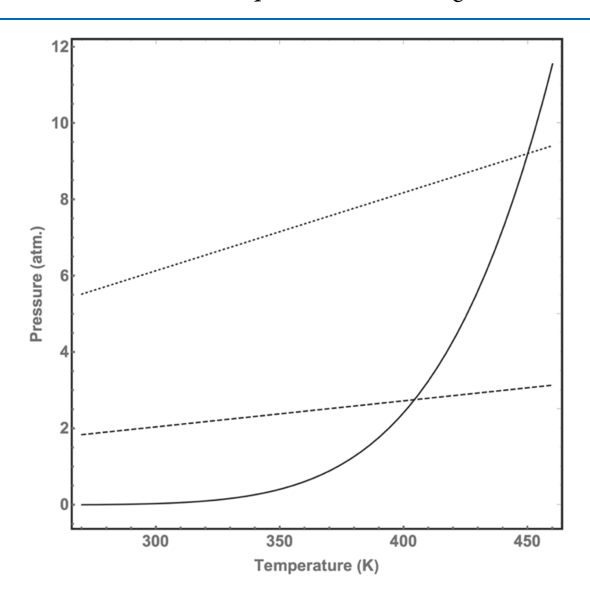


Figure 4. Vapor pressure (solid curve) of water and the pressure (dashed line) in the chamber as a function of temperature. The dotted line is the expected pressure in the chamber if the reactants are tripled.

the dashed line in Figure 4. The vapor pressure of water can be obtained with Hyland and Wexler's equation: ²¹

$$P_{\text{vapor}} = \exp\left[\frac{-0.58002206 \times 10^4}{T} + 1.3914993 - 0.048640239 T + 0.41764768 \times 10^{-4} T^2 - 0.14452093 \times 10^{-7} T^3 + 6.5459673 \ln(T)\right]$$
(6

with T in K and $P_{\rm vapor}$ in Pa as shown in Figure 4 with a solid curve. From Figure 4, we see that two curves cross at temperature 404.2 K, above which the pressure in the chamber is lower than the vapor pressure, most of the H_2O molecules will detach from the CoO surfaces and vice versa.

We may assume that the $[(H_2)^*]$ and $[(CO)^*]$ are proportional to the concentrations of adsorbed H_2O and CO_2 molecules on the CoO surface. The adsorbed CO_2 remained in the form of chemisorption, and its concentration is not very sensitive to the temperature, 3 while H_2O concentration is very sensitive to the temperature, considering the vapor pressure effect because of the physisorption. In the temperature range from 273 to 500 K, $[(CO)^*]$ is simply considered as a constant, while $[(H_2)^*]$ abruptly decreases above T_v due to evaporation; we may express $[(H_2)^*]$ with

$$[(H_2)^*] \propto \frac{1}{e^{(T-T_v)/b} + 1} + d$$
 (7)

d is the portion of $[(H_2)^*]$ comparing to temperature lower than T_{v_i} b describes the temperature range in which water evaporates. Eq 7 indicates that when temperature is lower than T_{v_i} $[(H_2)^*]$ is a constant and is a different constant if the temperature is higher than T_{v_i} as shown in Figure 6. The reaction rate of eq 4 is calculated by

$$r(T) = Ce^{-(E_a/k_BT)} \left(\frac{1}{e^{(T-T_v)/b} + 1} + d \right)^m$$
(8)

where *C* is a constant.

r(T) is proportional to the amount of hydrocarbon products. As shown in Figure 2, all the alkane products show almost the same temperature dependence. The total alkane hydrocarbon products are calculated from Figure 2 by adding all the hydrocarbons from heptane to hexadecane and neglecting other hydrocarbons. The temperature dependence of the total alkane hydrocarbon products is shown in Figure 5 with dots. With eq 8, theoretical fitting to the experimental results is performed and shown with a dashed curve in Figure 5, where the peak of production rate is calculated to be at 402.5 K. We found that with the parameters $E_a = 1.1 \text{ eV}$, $T_v = 404.5 \text{ K}$, b =0.7K, d = 0.4%, and m = 1, the calculation fits to the experimental data. E_a , the activation energy, is 1.1 eV, which is in agreement with the one for hydrocarbon formation from CO and H_2 . ^{22–26} $T_v = 404.5$ K is almost the same as the value estimated with the ideal gas state equation and the Hyland and Wexler's equation in the above and is little bit higher than 402.5 K at which the production is at maximum. That b = 0.7Krepresents that within a narrow temperature range of 0.7 K, the adsorbed H_2O were released from the catalyst. That d = 0.4%represents the remaining amount of H₂O left on the CoO surface above T_v . Here, we have set m = 1 for simplicity since the model is insensitive to this fitting parameters. With the fitting parameters, eq 7 is plotted in Figure 6, where the concentrations above and below $T_{\rm v}$ are almost constants. In reality, they are not constants but a function decreasing with the temperature increasing. ^{18–20} Taking this into account, the underestimation at temperature lower than 360 K and overestimation at about 490 K as shown in Figure 5 might be improved. However, as shown in the inset of Figure 5, the experimental value at about 330 K is more than 10 times larger than that of the calculation with eq 8. This cannot be simply explained by the present model, which needs further study.

From Figure 4, we see that $T_{\rm v}$ increases with more reactants. For example, if the reactants are tripled, as shown with the dotted line, then $T_{\rm v}$ is expected to increase to about 450 from 404.5 K, and the reaction rate will increase by 20 times according to eq 5.

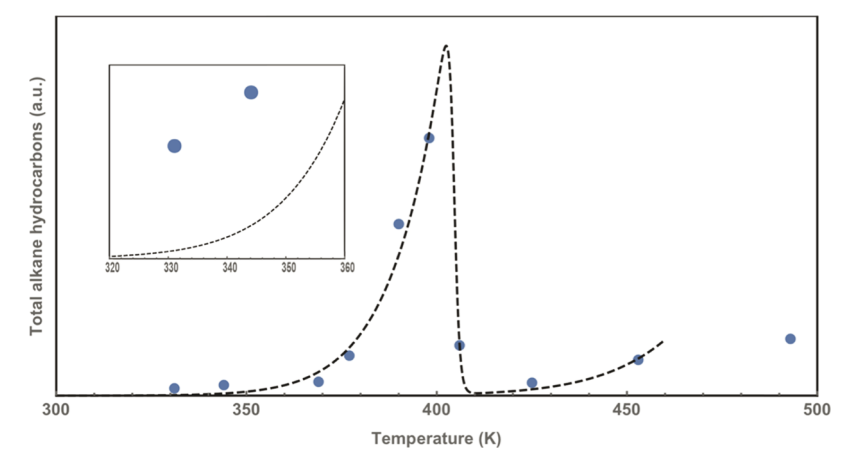


Figure 5. Temperature dependence of total alkane hydrocarbons obtained from Figure 2. Dots are experimental results, and the dashed curve is the theoretical fitting with eq 8. The inset shows a large disagreement between the experimental data and the calculated result in a lower temperature range.

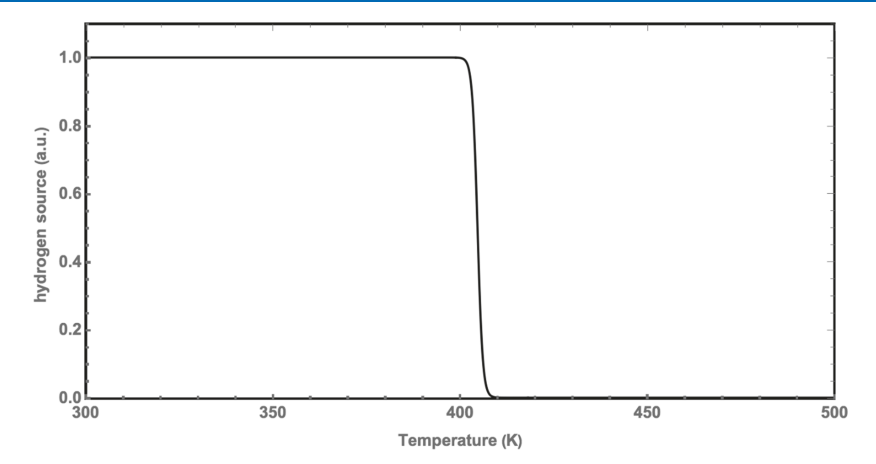


Figure 6. Calculated hydrogen source as a function of temperature.

Figure 2 shows that alkane hydrocarbon production decreases when temperature increases from 220 to 242 °C, while other kinds of hydrocarbons appear. As shown in Figures 1 and 3, benzene (C₆H₆) and benzene derivatives such as toluene (C_7H_8) , p-xylene (C_8H_{10}) , and C_9H_{12} will form. At a higher temperature, the hydrogen source is very low while carbon source remains the same because of the chemisorption, and thus benzene and its derivatives with low hydrogen atom number tend to form. However, converting alkanes into aromatic hydrocarbons might be another mechanism for the explanation to the phenomenon, ^{27–29} i.e., chain hydrocarbons were synthesized before converting to benzene (C₆H₆) and benzene derivatives. The conversion generally happens at a temperature higher than 500 $^{\circ}$ C, ^{27–29} but the temperature in the present experiment is only about 240 °C that is too low for the conversion to happen. The experimental result shows that the CoO/Co surface can also be used as a catalyst to form benzene and benzene derivatives by controlling temperature and the relative ratio between carbon and hydrogen sources, which needs further studies.

3. CONCLUSIONS

The experimental results show that chain hydrocarbons (C_nH_{2n+2}) where $3 \le n \le 16$ mainly form at a temperature higher than about 60 °C, and the production rate reaches a maximum at 130 °C, abruptly decreases above 130 °C, and

then gradually increases until 220 °C; while the temperature is higher than 220 °C, benzene (C₆H₆) and benzene derivatives such as toluene (C₇H₈), p-xylene (C₈H₁₀), and C₉H₁₂ form. The modeling of temperature dependence of the reaction rate reveals that the vaporization of the adsorbed water contributes to the sharp peak; the activation energy is estimated as about 1 eV, which is in agreement with the reaction of CO and H₂ to synthesize chain hydrocarbons. The experimental results support the mechanism that the chemisorbed CO2 and physisorbed H₂O on the CoO surface are disassociated or excited with light; the disassociated or excited molecules then synthesize hydrocarbons. When most of the water molecules leave from the CoO at a temperature higher than 220 °C, the hydrogen source is depleted, while the carbon source remains the same due to chemisorption, and thus benzene and its derivatives with low hydrogen atom number could form. Due to H₂O vaporization, higher pressure in the chamber leads to a higher reaction rate.

4. EXPERIMENTAL SECTION

The cobalt (Co) powder was obtained from Goodfellow. The diameters of the Co micro-particles are in the range of 50-100 μm . The Co micro-particles were mixed with a 3.5% aqueous solution of hydrogen chloride (HCl) for 10 min then rinsed with distilled water. The oxide layered structures were removed from the Co particle surfaces by acid etching. The catalyst was

then degassed in vacuum for approximately 1 h to remove the carbon dioxide adsorbed on the surfaces. Nanoflakes were then formed on the particle surfaces after placing the Co powder in air at room temperature for 2 h. This method was reported in previous articles. This sample preparation is cost effective, comparing the method with a femtosecond laser irradiation in water. Two grams of catalyst was loaded in a glass reactor (20 mL), and 350 mg of distilled water was added into the reactor to cover the catalyst. Afterward, the reactor was evacuated to about 1×10^{-3} atm and then filled with $\rm CO_2$ to an absolute pressure of 2 atm at a room temperature of about 20 °C.

The glass reactor was placed horizontally and manually shook so that the cobalt particles spread uniformly on the bottom half of the cylindrical wall of the reactor. A solar lamp for simulating natural sunlight (Honle, SOL 500) was used to irradiate the nanostructured Co micro-particles in the sealed reactor. During the irradiation, the reactor was laid on a stage with a tilt angle of 10° to the stage surface below the solar lamp, which is crucial for this experiment. If the reactor was laid down horizontally perfectly, during the irradiation, the water vapor will condensate near the cap easily, which makes the cobalt particles too dry to react. Tilting reactors allow condensed water to flow back to the cobalt particles and keep them wet. The distance between the solar lamp and the glass vial was 15 cm so that the light intensity is 100 mW/cm², which is similar to the sunlight intensity. About half of the cylinder glass reactor was wrapped with different materials to keep the cobalt particles at different temperatures but in the same light intensity.³⁻⁵ In this experiment, fiberglass, paper, rubber, and aluminum sheet were used to keep the reactor at different temperatures. For temperatures higher than 200 °C, an electric heating plate was used along with an extra heat source because only light at 100 mW/cm² cannot heat the sample to a temperature higher than 200 °C in the present simple reactor setup. Thermal couples were attached to the bottom half of the reactor to monitor the temperature. A control experiment was also conducted with the same experimental setup except no light irradiation to know if there are any contaminations.

After 20 h of irradiation, the products were extracted with approximately 3 mL of dichloromethane (DCM), which was injected into the reactor to extract non-volatile organic products. The DCM extract was then analyzed using a Bruker Scion SQ gas chromatography—mass spectrometry (GC–MS) with a 30 m ZB-624 capillary column.

AUTHOR INFORMATION

Corresponding Author

Mengyan Shen – Department of Physics and Applied Physics, University of Massachusetts Lowell and Nanomanufacturing Center, University of Massachusetts Lowell, One University Avenue, Lowell, Massachusetts 01854, United States;

orcid.org/0000-0001-9884-4815; Email: Mengyan_Shen@uml.edu

Authors

Haizhou Ren – Department of Physics and Applied Physics, University of Massachusetts Lowell, One University Avenue, Lowell, Massachusetts 01854, United States

Zhe Kan – Department of Physics and Applied Physics, University of Massachusetts Lowell, One University Avenue, Lowell, Massachusetts 01854, United States Zibo Wang — Department of Physics and Applied Physics, University of Massachusetts Lowell, One University Avenue, Lowell, Massachusetts 01854, United States

Complete contact information is available at: https://pubs.acs.org/10.1021/acsomega.0c04693

Author Contributions

H.R. and M.S. conceived the idea for the project. H.R. prepared samples and performed the hydrocarbon synthesis experiments. H.R., Z.K., and Z.W. analyzed the synthesized products. H.R., Z.K., Z.W., and MS. discussed the results, analyzed the data, and drafted the manuscript. M.S. finalized the manuscript.

Notes

The authors declare no competing financial interest. The data that support the findings of this study are available from the corresponding author upon reasonable request.

ACKNOWLEDGMENTS

We thank Dr. M. Zheng and Dr. M. Jayamanna for experimental assistance and Dr. C. Wang and Dr. L. Li for helpful discussions. This research was supported by the National Science Foundation (CHE-1836540).

REFERENCES

- (1) Wang, C.; Shen, M.; Huo, H.; Ren, H.; Yan, F.; Johnson, M. Nature-like photosynthesis of water and carbon dioxide with femtosecond laser induced self-assembled metal nanostructures. *Int. J. Mod. Phys. B* **2009**, 23, 5849–5857. , Erratum: 2014, 1492004.
- (2) Wang, C.; Shen, M.; Huo, H.; Ren, H.; Johnson, M. Using metal nanostructures to form hydrocarbons from carbon dioxide, water and sunlight. *AIP Adv.* **2011**, *1*, No. 042124.
- (3) Wang, C.; Ren, H.; Zeng, M.; Zhu, Q.; Zhang, Q.; Kan, Z.; Wang, Z.; Shen, M.; Acharige, M. J. T.; Ruths, M.; Ryan, D. K.; Li, G.; Kolesov, G.; Kaxiras, E.; Mazur, E. Low-cost visible-light photosynthesis of water and adsorbed carbon dioxide into long-chain hydrocarbons. *Chem. Phys. Lett.* **2020**, 739, 136985.1–136985.6.
- (4) Zhu, Q.; Wang, C.; Ren, H.; Zeng, M.; Kan, Z.; Wang, Z.; Shen, M. Conversion of Water and Carbon Dioxide into Methanol with Solar Energy on Au/Co Nanostructured Surfaces. *Mater. Res. Express* **2020**, *7*, 35014.
- (5) Zeng, M.; Kan, Z.; Wang, Z.; Shen, M. Carbon isotope effects in the artificial photosynthesis reactions catalyzed by nanostructured Co/CoO. *Chem. Phys. Lett.* **2020**, *754*, 137731.1–137731.137731.
- (6) Visconti, C. G.; Lietti, L.; Tronconi, E.; Forzatti, P.; Zennaro, R.; Finocchio, E. Fischer—Tropsch synthesis on a Co/Al₂O₃ catalyst with CO₂ containing syngas. *Appl. Catal. A* **2009**, 355, 61–68.
- (7) Gnanamani, M. K.; Shafer, W. D.; Sparks, D. E.; Davis, B. H. Fischer–Tropsch synthesis: Effect of CO_2 containing syngas over Pt promoted Co/γ -Al₂O₃ and K-promoted Fe catalysts. *Catal. Commun.* **2011**, *12*, 936–939.
- (8) Tachibana, Y.; Vayssieres, L.; Durrant, J. R. Artificial photosynthesis for solar water-splitting. *Nat. Photonics* **2012**, *6*, 511–518.
- (9) Mukherjee, S.; Libisch, F.; Large, N.; Neumann, O.; Brown, L.; Cheng, J.; Lassiter, J.; Carter, E.; Nordlander, P.; Halas, N. Hot Electrons Do the Impossible: Plasmon-Induced Dissociation of H₂ on Au. *Nano Lett.* **2013**, *13*, 240–247.
- (10) Grossman, J. C.; Schwegler, E.; Draeger, E. W.; Gygi, F.; Galli, G. Towards an assessment of the accuracy of density functional theory for first principles simulations of water. *J. Chem. Phys.* **2004**, *120*, 300–311.
- (11) Xu, L.; Ma, Y.; Zhang, Y.; Chen, B.; Wu, Z.; Jiang, Z.; Huang, W. Water Adsorption on a Co(0001), Surface. *J. Phys. Chem. C* **2010**, *114*, 17023–17029.
- (12) Park, K.; Kolpak, A. M. Understanding photocatalytic overall water splitting on CoO nanoparticles: Effects of facets, surface

- stoichiometry, and the CoO/water interface. *J. Catal.* **2018**, 365, 115–124.
- (13) Park, K.-W.; Kolpak, A. M. Mechanism for spontaneous oxygen and hydrogen evolution reactions on CoO nanoparticles. *J. Mater. Chem. A* **2019**, *7*, 6708–6719.
- (14) NIST; https://webbook.nist.gov/cgi/cbook.cgi?Formula=+C9H12&NoIon=on&Units=SI.
- (15) Jayamanna, M. Hydrocarbon Production from CO2 and Water with Sunlight on Zero Valent Iron Nanoparticles; Ph.D. Dissertation, University of Massachusetts Lowell: 2017.
- (16) Muller, P. Glossary of terms used in physical organic chemistry (IUPAC Recommendations 1994). *Pure Appl. Chem.* **1994**, *66*, 1077–1184.
- (17) Arrhenius, S. Über die Dissociationswärme und den Einfluss der Temperatur auf den Dissociationsgrad der Elektrolyte. Z. Phys. Chem. 1889, 4, 96–116.
- (18) Petitto, S. C.; Marsh, E. M.; Carson, G. A.; Langell, M. A. Cobalt oxide surface chemistry: The interaction of $CoO(1\ 0\ 0)$, $Co_3O_4\ (1\ 1\ 0)$, and $Co_3O_4\ (1\ 1\ 1)$ with oxygen and water. *J. Mol. Catal. A: Chem.* **2008**, 281, 49–58.
- (19) Peixinho, J.; Lefèvre, G.; Coudert, F.-X.; Hurisse, O. Water evaporation in silica colloidal deposits. *J. Colloid Interface Sci.* **2013**, 408, 206–211.
- (20) Findenegg, G.H. Principles of Adsorption at Solid Surfaces and their Significance in Gas/Solid and Liquid/Solid Chromatography. *Theoretical Advancement in Chromatography and Related Separation Techniques*; NATO ASI Series (Series C: Mathematical and Physical Sciences) Vol 383, Springer: Dordrecht, 1992; pp. 227–260.
- (21) Hyland, R. W.; Wexler, A. Formulations for the thermodynamic properties of the saturated phases of H₂O from 173.15 K to 473.15 K. ASHRAE Trans. 1983, 89, 500–519.
- (22) Nikparsaa, P.; Mirzaeia, A. A.; Atashi, H. Effect of reaction conditions and Kinetic study on the Fischer-Tropsch synthesis over fused Co-Ni/Al₂O₃ catalyst. *J. Fuel Chem. Technol.* **2014**, 42, 710–718.
- (23) Arsalanfar, M.; Mirzaei, A. A.; Atashi, H.; Bozorgzadeh, H. R.; Vahid, S.; Zare, A. An investigation of the kinetics and mechanism of Fischer-Tropsch synthesis on Fe-Co-Mn supported catalyst. *Fuel Process. Technol.* **2012**, *96*, 150–159.
- (24) Yates, I. C.; Satterfield, C. N. Intrinsic kinetics of the Fischer-Tropsch synthesis on a cobalt catalyst. *Energy Fuels* **1991**, *5*, 168–173. (25) Subiranas, A.M. *Combining Fischer-Tropsch Synthesis (FTS) and*
- (25) Subiranas, A.M. Combining Fischer-Tropsch Synthesis (FTS) and Hydrocarbon Reactions in one Reactor; Ph.D. Dissertation, Universität Karlsruhe, Karlsruhe, 2008.
- (26) Zennaro, R.; Tagliabue, M.; Bartholomew, C. H. Kinetics of Fischer—Tropsch synthesis on titania-supported cobalt. *Catal. Today* **2000**, *58*, 309–319.
- (27) Gnep, N. S.; Doyemet, J. Y.; Seco, A. M.; Ribeiro, F. R.; Guisnet, M. Conversion of light alkanes into aromatic hydrocarbons: 1-dehydrocyclodimerization of propane on PtHZSM-5 catalysts. *Appl. Catal.* **1987**, *35*, 93–108.
- (28) Gnep, N. S.; Doyemet, J. Y.; Guisnet, M. Conversion of Light Alkanes Into Aromatic Hydrocarbons. 3. Aromatization of Propane and Propene on Mixtures of HZSM5 and of Ga₂O₃. *Stud. Surf. Sci. Catal.* **1989**, *46*, 153–162.
- (29) Migliori, M.; Aloise, A.; Catizzone, E.; Caravella, A.; Giordano, G. Simplified Kinetic Modeling of Propane Aromatization over Ga-ZSM-5 Zeolites: Comparison with Experimental Data. *Ind. Eng. Chem. Res.* **2017**, *56*, 10309–10317.
- (30) Kan, Z.; Zhang, Q.; Ren, H.; Shen, M. Femtosecond laser induced formation of graphene nanostructures in water and their field emission properties. *Mater. Res. Express* **2019**, *6*, No. 085016.
- (31) Kan, Z.; Zhu, Q.; Ren, H.; Shen, M. Femtosecond Laser-Induced Thermal Transport in Silicon with Liquid Cooling Bath. *Materials* **2019**, 2043, 1–2043.14.
- (32) Shen, M. Y.; Crouch, C. H.; Carey, J. E.; Mazur, E. Femtosecond laser-induced formation of submicrometer spikes on silicon in water. *Appl. Phys. Lett.* **2004**, *85*, 5694–5696.

(33) Shen, M.; Carey, J. E.; Crouch, C. H.; Kandyla, M.; Stone, H. A.; Mazur, E. High-density regular arrays of nanometer-scale rods formed on silicon surfaces via femtosecond laser irradiation in water. *Nano Lett.* **2008**, *8*, 2087–2091.